STATIC TESTER FOR CHARACTERIZATION OF OPTICAL NEAR-FIELD COUPLING PHENOMENA

Ferry Zijp*), Yourii V. Martynov

Philips Research Laboratories
Prof. Holstlaan 4, 5656AA Eindhoven, The Netherlands

ABSTRACT

We present an experimental set-up for systematical studies of optical near-field coupling phenomena using a solid immersion lens (SIL) to surpass the conventional far field diffraction limit. The set-up incorporates a microscope objective lens with NA=0.80 in combination with a hemispherical SIL manufactured from glass with refractive index n=1.887 and a laser with a wavelength of 430 nm. Test samples are positioned within the evanescent decay distance from the bottom surface of the SIL using a closed-loop-controlled piezo actuator. The laser spot can be scanned over the sample enabling a study of the push-pull signal of pregrooved samples on a split photodiode. The intensity distribution and polarisation state of the light reflected from the sample in the exit pupil of the microscope objective lens is studied on a CCD camera. The reflected light can be combined with a reference beam into an interferogram used for alignment purposes. We present measurements of evanescent coupling of light to a glass sample and the push-pull signal of a reflective phase grating with a groove pitch of 300 nm as a function of thickness of the air gap between de SIL and the sample. The evanescent coupling to a glass sample can accurately be described by thin-film optics theory. Experiments show that the push-pull signal amplitude depends on the polarisation state of the irradiating beam.

Keywords: near-field, evanescent field, solid immersion lens

1. INTRODUCTION

Near-field optical recording is a promising new data storage technology. An important part of a near-field optical recording system is a solid immersion lens (SIL) that is used to increase the numerical aperture of the irradiating objective lens by a maximum factor of the refractive index n of the SIL. Such a combination of objective lens and SIL can result in an effective numerical aperture larger than 1. For read-out using the full effective numerical aperture, the medium must be close to the bottom surface of the SIL within the evanescent decay distance of the light (the near-field) that is focussed at an angle larger than the critical angle. This evanescent decay distance is a fraction of the wavelength of the irradiating laser beam. Practical near-field recording systems rely therefore on an air-bearing slider to maintain this distance. Slider technology, however, does not provide sufficient freedom in changing the air gap and the speed of the lateral movement of the medium to allow for a systematic experimental study of the phenomena that are related to near-field coupling and diffraction by grooves and recording layers. Besides the technological challenges of building a fully functional near-field optical recorder system, the system requires thorough theoretical investigation. Whereas conventional far-field optical recording systems such as CD and DVD can quite accurately be described by scalar or quasi-vectorplane wave theory, near-field optics requires a full vector approach.

To improve the understanding of the above phenomena we have built a near-field static tester. In this experimental set up we use a piezo actuator rather than a slider to position a test sample with respect to the bottom surface of the SIL in a reproducible way with nanometer precision.

*) Correspondence: E-mail: Ferry.Zijp@philips.com

In *Optical Storage and Optical Information Processing*, Han-Ping D. Shieh, Tom D. Milster, Editors, Proceedings of SPIE Vol. 4081 (2000) • 0277-786X/00/$15.00

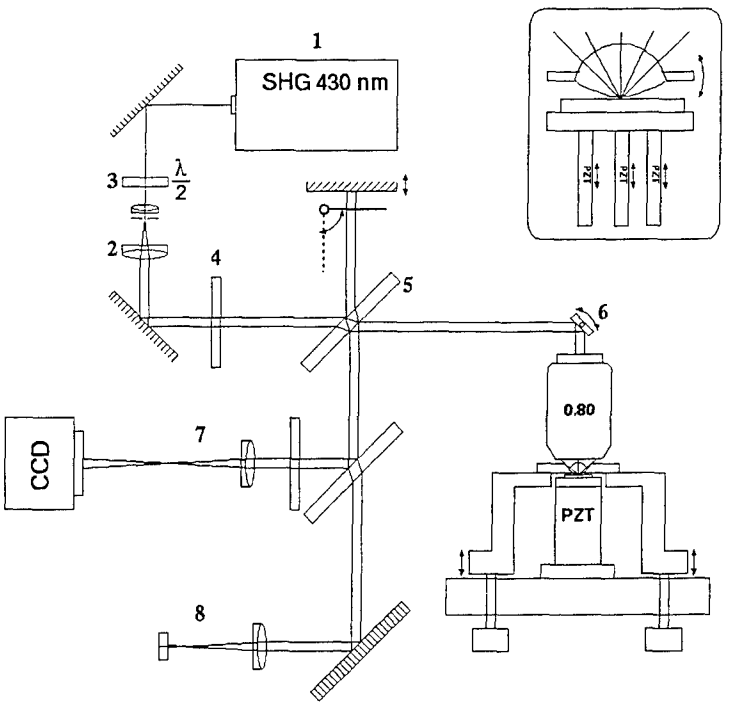

Figure 1. Diagram of the near-field static tester.

2. NEAR-FIELD STATIC TESTER

2.1 Experimental set-up

The experimental set-up is depicted in Figure 1. As a light source we used a continuous-wave frequency-doubled diode laser (1) with a wavelength of 430 nm. The laser beam is expanded by a telescope (2) with spatial filter to reduce aberrations and create a parallel beam with a homogeneous intensity distribution. A half-wave plate (3) is used to select a polarisation state and an additional polariser (4) eliminates any residual ellipticity. A beam splitter plate (5) reflects a portion of the beam towards a reference mirror while the rest of the beam is directed into the optical head. A galvano mirror (6) is used to scan the optical spot over a test sample. Light reflected from the sample is analysed by two detection branches (7) and (8). In the first branch (7) the exit pupil of the microscope objective lens is imaged onto a CCD camera in order to study the intensity distribution and the polarisation state of the reflected light. In the second branch (8) light is detected with a split photo diode generating push-pull signal. In order to suppress parasite signals the lens in this branch is positioned in such a way that the scanning galvano mirror and the photodetector are in its conjugate planes

The set-up incorporates a large-working-distance microscope objective lens with NA=0.80 in combination with a hemispherical SIL manufactured from the LASFN-9 glass sort that has refractive index n=1.887 at 430 nm. The first surface of the SIL was antireflection coated while its bottom is bare. The sample is mounted on top of a piezo actuator. The actuator contains 3 piezo elements that can be controlled in closed loop using built-in strain gauge displacement sensors. The actuator allows adjustment of tip-tilt and translation along the optical axis with accuracy better than 1 nm. The SIL is fixed in a holder in a form of a cap covering the actuator and can be aligned using three micro spindles. The SIL holder is made from the same material as the actuator body (stainless steel) in order to minimise displacements due to thermal expansion. The current set-up does not include a direct measurement of the distance between SIL and the sample. Therefore, we measure the sample displacement relative to the position of mechanical contact which can be determined with an accuracy of approximately 5 nm by observing changes in the CCD image while the sample is moving continuously towards SIL.

2.2 Alignment of the SIL head

We chose a hemispherical SIL instead of the super-spherical SIL because of its more relaxed tolerance on the thickness. The choice of the shape of bottom surface of the SIL was determined by the alignment problem. For a flat bottom the tolerance on angular alignment of the SIL and a flat sample for very small air gaps becomes prohibitively tight. To overcome this problem several solutions have been proposed ranging from conical bottoms with a sharp tip [1], a very small 'nose' [2] to a spherical bottom surface [3]. We have chosen to grind and polish the bottom surface spherically because such a geometry has a contact point at any tilt angle between SIL and test sample. In such a geometry alignment is only necessary to reduce aberrations by making sure that this contact point lies within the field of view of the objective-SIL combination. In order to be able to determine the angle between the SIL and the sample, the SIL was mounted in a small glass disk with its optical axis perpendicular to the disk surface. By irradiating the sample with a parallel laser beam through this disk we could obtain an interference pattern between the light reflected from the test sample and the surface of this small disk facing the test sample (the surface of the disk facing the irradiating laser beam is antireflection coated). By minimising the number of tilt-fringes of the interference pattern the SIL can be aligned with respect to the sample within 0.1 mrad. After aligning the SIL to the sample, the microscope objective lens is put into place. By moving the objective lens in two lateral directions and monitoring the image on the camera the contact point between SIL and the sample can be found. Another way of aligning the optical axis of the objective lens with the optical axis of the SIL is by minimising the astigmatism that is induced by misalignment.

3. EXPERIMENTAL RESULTS

3.1 Evanescent coupling to a glass sample

With the static tester set-up we studied evanescent coupling of light to a bare glass sample with refractive index n=1.48 by measuring the amount of reflected light with a single photodiode at the position of the push-pull detector and by analysing the intensity distribution and polarisation state in the image of the exit pupil of the objective lens on the CCD camera. The experimental results were compared with simulations using the classical thin-film matrix formalism. This specific configuration with evanescent coupling to bare dielectric is relevant for the case of lithographic production of optical disk masters using a SIL. Near-field mastering systems have been proposed that control the SIL-to-master-disk distance with an actuator. The total amount of reflected light might serve as the error signal for the air gap servo in such a system [4].

In Figure 2 we show images of the reflected light intensity distribution recorded with the CCD camera for an air gap of 1000 nm and the axis of the analyser parallel (a) and perpendicular (b) to the polarisation direction of the irradiating beam. In Figures 2 (c) and (d) the simulated intensity distributions for the same polarisation states are shown. As can be seen from these images the rays that are focussed at angles larger than the critical angle are totally internal reflected at the bottom of the SIL, hence the bright ring outside NA=1. There is no evanescent coupling to the glass sample for this large air gap, only the rays within NA=1 propagate to the glass sample. The multiple reflections between the glass sample and the bottom of the SIL cause the interference pattern in the reflected light within NA=1. These concentric fringes may be used to align the optical axes of the objective lens and SIL. We also observe that, in agreement with theory, part of the reflected light has changed polarisation state from horizontal to vertical, most notably the parts of the pupil that are focussed at large angles to the bottom of the SIL since for the larger angles the difference between the Fresnel reflection coefficients for s and p polarisation is largest.

In Figure 3 we show images of the reflected light intensity distribution recorded with the CCD for an air gap of 100 nm and the axis of the analyser parallel (a) and perpendicular (b) to the polarisation direction of the irradiating beam. Figures 3 (c) and (d) depict simulated intensity distributions for the same polarisation states. In these images the bright ring at NA>1 has disappeared since the larger part of the light is transmitted into the glass sample by evanescent coupling.

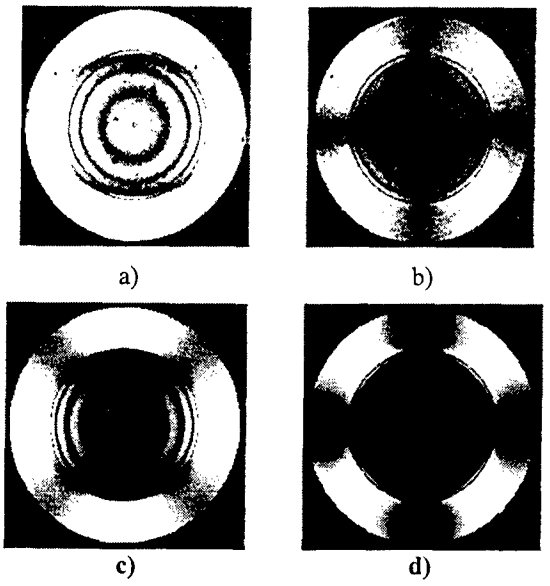

Figure 2. Images of the reflected light intensity distribution for an air gap of 1000 nm and the axis of the analyser parallel (a) and perpendicular (b) to the polarisation of the irradiating beam. In (c) and (d) the simulated intensity distributions are shown for the same polarisation states.

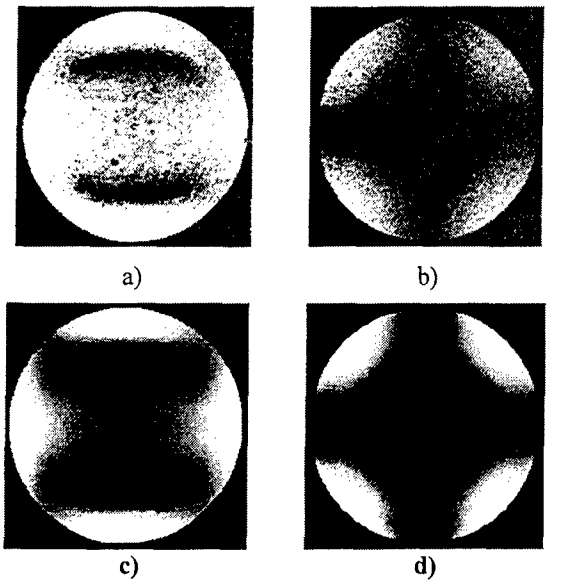

Figure 3. Images of the reflected light intensity distribution for an air gap of 100 nm and the axis of the analyser parallel (a) and perpendicular (b) to the polarisation of the irradiating beam. In (c) and (d) the simulated intensity distributions are shown for the same polarisation states.

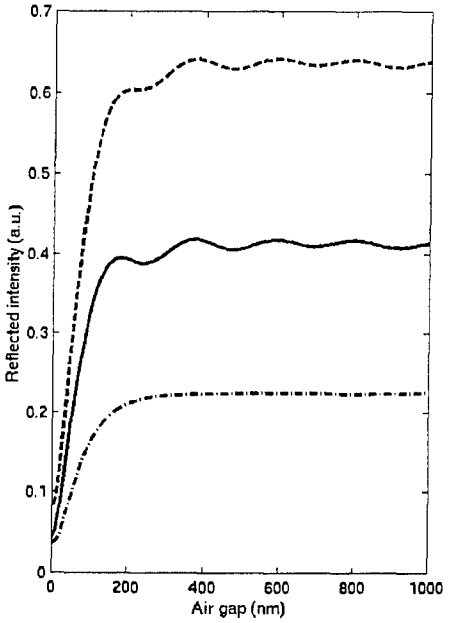

Figure 4. Simulation of the total amounts of the reflected light for the polarisation states parallel (—) and perpendicular (---) to the polarisation state of the irradiating beam, and the sum of both (--).

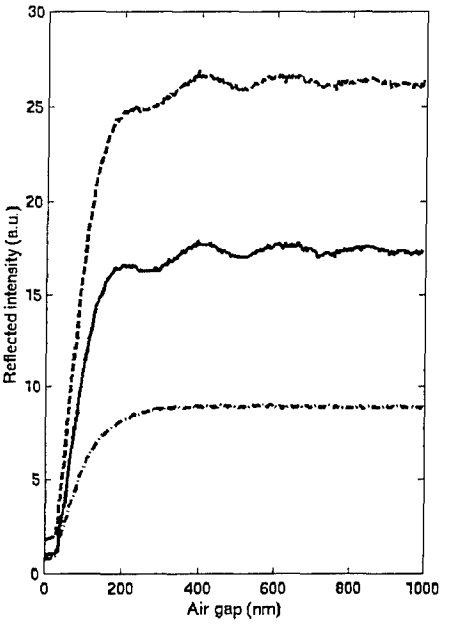

Figure 5. Measurement of the total amounts of the reflected light for the polarisation states parallel (—) and perpendicular (---) to the polarisation state of the irradiating beam, and the sum of both (--).

In Figures 4 and 5 we show the simulation and measurement of the total amounts of the reflected light for both polarisation states and the sum of both. These measurements were corrected for the reflection coefficients of the beam splitter for s and p polarisation. The measurements are in good agreement with theory, the evanescent coupling becomes perceptible below 200 nm and the total reflection drops almost linearly to a minimum at contact. This linear signal may be used as an error signal for a closed loop servo system of the air gap. The oscillations in the horizontal polarisation are caused by the reduction of the number of fringes within NA=1 (see Figure 2) with decreasing of the gap thickness.

3.2 Near-field coupling to a pregrooved disk

In the same setup we also studied reflective phase grating samples resembling portions of a pregrooved disc. The grating was written in a photoresist layer using an UV optical disc mastering machine. A 30 nm layer of aluminium was deposited on top of the grating after development. The resulting sample had a groove pitch of 300 nm, 50% duty cycle and a groove depth of 80 nm. The samples were mounted with the aluminium layer facing SIL.

In Figure 6 the CCD images are shown at air gaps of 750 nm, 250 nm and 40 nm for irradiation with the polarisation perpendicular to the grooves. At the large gap of 750 nm the $+1^{st}$ en -1^{st} diffracted order can bee seen clearly within NA=1. The ring outside NA=1 is due to the total internal reflection at the bottom of the SIL. At an air gap of 250 nm the edges of the diffracted orders appear less sharp because of partial evanescent coupling of light at NA>1. At even smaller air gaps the edges become sharp again since most of the light at NA>1 is coupled to the grooves and, upon diffraction, is returned back into SIL. At a distance of 40 nm the diffracted orders fill the entire pupil, at this distance almost the full effective numerical aperture of 1.51 is reached.

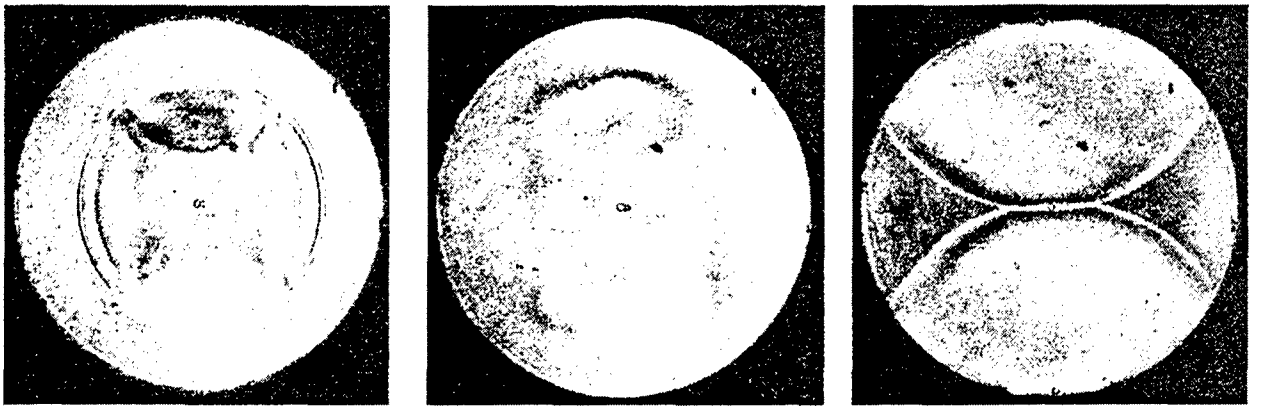

a) b) c)

Figure 6. CCD images at an air gap of 750 nm (a), 250 nm (b) and 40 nm (c) for irradiation with the polarisation perpendicular to the grooves.

3.3 Push-pull signals

We measured the amplitude of the push-pull signal from the split photodiode with the focussed spot scanning perpendicular to the grooves of the above described pregrooved sample by driving the galvano mirror with an AC current. The push-pull signal we measured was the difference signal from the two split photodiode signals. The push-pull signal was not normalised to the sum of the signals as is usually done in practical optical storage systems. A sample of the push-pull signal for an air gap thickness equal to 20 nm is shown in Figure 7. In Figure 8 the push-pull signal is plotted versus the air gap with the polarisation of the irradiating beam perpendicular to the grooves and in Figure 9 parallel to the grooves. The procedure we used to determine the maximum push-pull signal was to move the test sample to a defined distance from the SIL and then determine the focus position at which maximum push-pull signal occurs. At larger air gaps we often found a strong push-pull at more than one focus position. A plausible explanation for this phenomenon is that aberrations caused by the objective lens, the SIL and also the air gap can be balanced with some defocus. Apart from the amount of defocus that yields a maximum push-pull signal, there may be other focus positions that result in a local maximum of the push-pull signal. Since the aberrations caused by the objective lens and the SIL and the air gap scale with the effective numerical aperture, and the amount of defocus at a certain focus position scales with the effective numerical aperture, the optimal focus position is not a constant but also varies as the air gap changes. The push-pull amplitude plotted in Figures 7 and 8 is the largest amplitude we found by choosing the optimal focus position at a given air gap. At air gaps larger than 300 nm the push-pull signal became very small so we limited the range of air gaps between 0 and 300 nm.

Both plots show that the push-pull amplitude decreases with increasing air gap size. This is readily understood since the modulation transfer function of the system deteriorates as the air gap thickness increases. There is, however, a difference between both plots. The push-pull signal does not appear to decrease between 100 and 200 nm air gap size when the polarisation of the irradiating beam is perpendicular to the grooves. So far, we do not have an explanation for this behaviour, it may be caused by the polarisation state alone, it might also be caused by aberrations from the objective lens, the SIL and the air gap. More detailed experiments are needed to gain a clearer picture of the influence of polarisation on the push-pull signal in the near-field regime.

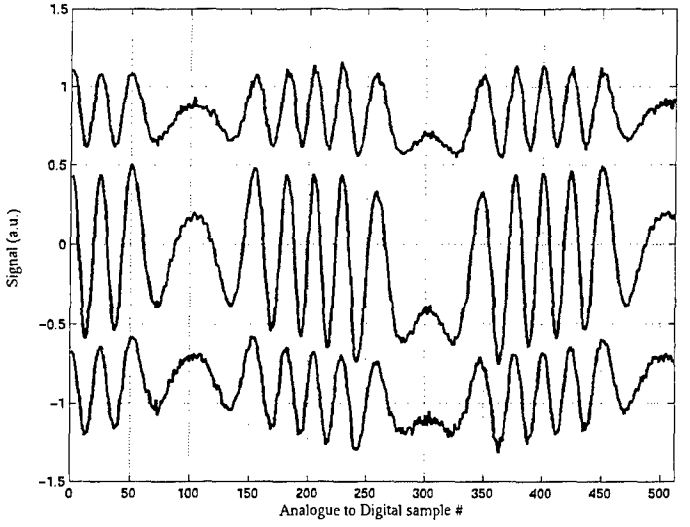

Figure 7. Push-pull signal at an air gap of 20 nm for polarisation of the irradiating beam perpendicular to the grooves. The push-pull signal (middle) is generated from the sum of one part of the split photodiode (upper signal) and the inverted signal of the other part (lower signal).

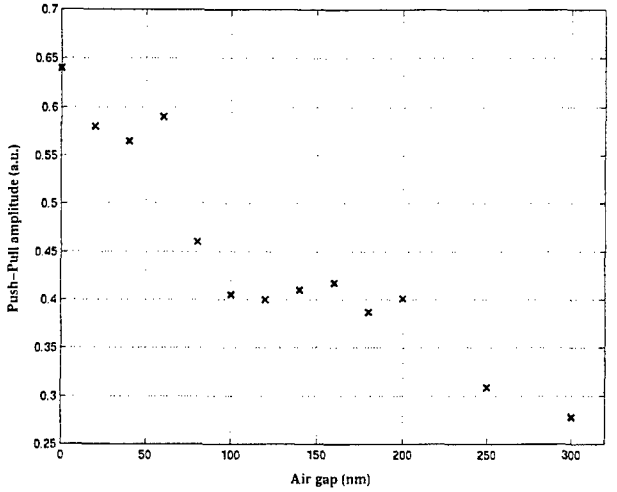

Figure 8. Measured push-pull signal versus the air gap with the polarisation of the irradiating beam perpendicular to the grooves.

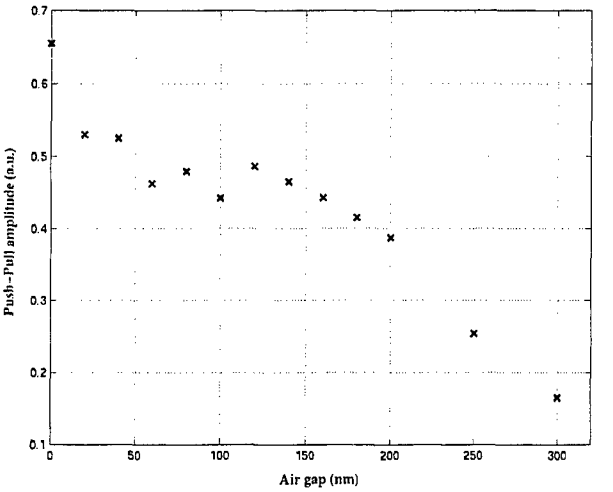

Figure 9. Measured push-pull signal versus the air gap with the polarisation of the irradiating beam parallel to the grooves.

4. CONCLUSION

We have built a near-field static tester set up equipped with a blue, 430 nm wavelength laser, a hemispherical solid immersion lens for systematic analysis of near-field related optical phenomena. In the system an effective numerical aperture of 1.51 can be achieved within a fraction of the evanescent decay length. Experiments show evanescent coupling to a glass sample that can well be described with classical thin-film theory. The push-pull signal from a reflective sample with 300 nm grooves has been measured as a function of air gap thickness. The Push-pull amplitude decreases as the air gap increases due to deterioration of modulation transfer function of the system. The Push-pull amplitude is also a function of the direction of polarisation of incident light.

5. ACKNOWLEDGEMENTS

The authors gratefully acknowledge Mr. C. Adema for his craftsmanship and ideas for fabricating and mounting the SIL, Ir. H. Goossens for his perfectly stable design of the SIL-head mechanics that hold the piezo and enable SIL to sample alignment and Dr. W. Koppers and Mr. G. van de Looij for manufacturing the grating test samples.

6. REFERENCES

1. L.P. Ghislain, V.B. Elings, "Near-field scanning solid immersion microscope", *Applied Phyics Letters* **72**, pp. 2779-2781.
2. K. Hirota et.al. , "Nearfield Phase Change Optical Recording Using a GaP Hemispherical Lens", *Technical Digest ISOM/ODS* , 1999, pp. 361-363.
3. J.A.H. Stotz, M.R. Freeman, "A stroboscopic scanning solid immersion lens microscope", *Rev. Sci.Instrum.* **68**, pp. 4468-4477
4. S. Imanishi et.al., "Near Field Optical Head on Disk Mastering Process", *Technical Digest ISOM/ODS,* 1999, pp. 9-11.